Influence and Compensation of Inverter Voltage Drop in Direct Torque Controlled Four-Switch Three-Phase PM Brushless AC Drives

Khoa D. Hoang, *Student Member, IEEE*, Z. Q. Zhu, *Fellow, IEEE*, and Martin P. Foster

***Abstract*— This paper presents direct torque control methodology for a four-switch three-phase (FSTP) inverter fed permanent magnet (PM) brushless AC (BLAC) machine, with reference to a conventional six-switch three-phase (SSTP) inverter. It has been found that when derived from conventional voltage model flux estimation scheme, predicted stator flux imbalance may be caused by unbalanced inverter voltage drop in the FSTP inverter in which one phase winding is directly connected to DC link mid-point. Whilst this imbalanced problem does not adversely affect the performance of current model-based DTC, it causes significantly non-sinusoidal current waveforms and considerably unbalanced current magnitudes in voltage model-based DTC. A new compensation scheme taking into account the different forward voltage drop values in the switching device and the free-wheeling diode is proposed for the voltage model-based DTC to correct for stator flux imbalance via the addition of corrective voltages to flux equations. The proposed scheme has significantly improved the shape of current waveforms with satisfactory balanced magnitudes, total harmonic distortion and torque ripple factor, as verified by both simulation and experimental results. It has been shown that it is possible for a FSTP inverter to provide similar performance to a SSTP inverter when driving a PM BLAC machine.**

***Index Terms*— Brushless AC machine, direct torque control, flux estimation, four-switch there-phase inverter, permanent magnet machine.**

NOMENCLATURE

i_a , i_b , i_c	Phase currents (A).
i_α , i_β	Transformed ($\alpha\beta$) currents (A).
L_s	Stator inductance (H).
p	Number of pole pairs.
R_s	Stator phase resistance (Ω).
S_A , S_B , S_C	Instantaneous inverter switching states.
v_{an} , v_{bn} , v_{cn}	Phase-to-neutral voltages (V).
v_{a0} , v_{b0} , v_{c0}	Phase-to-zero voltages (V).
v_{n0}	Neutral-to-zero voltage (V).
v_α , v_β	Transformed ($\alpha\beta$) voltages (V).
T_e	Electromagnetic torque (N.m).
ψ_{sa} , ψ_{sb} , ψ_{sc}	Phase stator fluxes (Wb).
$\psi_{s\alpha}$, $\psi_{s\beta}$	Transformed ($\alpha\beta$) stator fluxes (Wb).
ψ_m	Permanent magnet flux linkage (Wb).
θ_e	Electrical rotor position (rad).
ω_e	Electrical rotor speed (rad/s).
*	Superscript indicating reference value.

Manuscript received 29 April, 2010; revised 6 July, 2010 and 24 September, 2010.

The authors are with the Department of Electronic and Electrical Engineering, The University of Sheffield, Sheffield S1 3JD U.K. (email: k.hoang@sheffield.ac.uk; k.d.hoang@ieee.org; z.q.zhu@sheffield.ac.uk; z.q.zhu@ieee.org; m.p.foster@sheffield.ac.uk).

Digital Object Identifier

I. INTRODUCTION

DIRECT torque and indirect torque control techniques are two common methodologies for controlling permanent magnet brushless AC machine [1], [2]. Normally, a six-switch three-phase (SSTP) inverter [Fig. 1(a)] is used for high performance operation of a three-phase machine and is almost universally considered the industry standard. For economic reasons, however, reducing the cost of the inverter is still under investigation and one obvious way to achieve this aim is to decrease the number of inverter switching devices.

Low cost inverter topologies with reduced number of switching devices for an induction machine drive system has been suggested and demonstrated in [3] and [4]. Welchko *et al.* [3] proposed using a three-switch three-phase inverter with an extra connection from neutral point to DC link mid-point to control torque and speed of an induction machine. Although this reduces the number of active switching devices, it requires modifications of both DC link and a specialized machine stator winding structure. A further disadvantage of this topology is that three phase currents are unidirectional and, hence, this topology is limited to particular applications. In [4] a four-switch three-phase (FSTP) inverter [Fig. 1(b)] was presented where one of three phase machine terminals was connected to the DC link mid-point and control achieved by manipulating the voltages and currents of the two active phases. The performance of this inverter was comparable to the traditional SSTP inverter. However, machines controlled by a FSTP inverter could only achieve half rated speed due to the fact that the voltage vector value is decreased by a factor of two in comparison with that in a conventional SSTP inverter drive system [5]. It should be noted that for an induction machine

drive system, reconfiguration of the windings from star to delta connection can allow full-speed operation [4]. Reduction in high order harmonic currents flowing in the mid-point connected phase current can be seen as a further benefit of the FSTP inverter topology. Other investigations on the FSTP inverter topology include the minimisation of torque ripple by applying space vector modulation schemes [6], the application of pulse width modulation (PWM) control methodologies to improve scalar PWM performance and DC link imbalance [7], and the elimination of current distortion at low-speed operation caused by the limited values of DC link capacitors using a compensation strategy [8]; it was also demonstrated that current waveforms under high-speed and inertial load conditions remain naturally balanced and sinusoidal without compensation [8].

Reliability improvement and fault tolerance are active areas of research for the FSTP topology. Fu *et al.* [9] introduced a control scheme to maintain operation of an induction machine fed from a SSTP inverter with a short-circuit fault in one inverter leg. The inverter was reconfigured from six switches to four and, according to the proposed fault isolation topology; performance of the entire drive system is maintained without significant disturbance as the drive system is reconfigured from a SSTP inverter to a FSTP inverter.

The drive systems briefly described above utilise the indirect torque control (ITC) methodology, the direct torque control (DTC) technique has also been developed with the FSTP inverter topology [10]. A conventional DTC SSTP inverter [11] requires eight stator voltage vectors. With a FSTP inverter, there are just four active switching states for DTC methodology without any zero voltage vectors [10]. As a result, only two-level hysteresis comparator is in use for both torque and flux control with a modified look-up table. An investigation of the FSTP inverter with DTC concept for fault tolerant control was carried out in [12] where it was proven that the DTC scheme achieves higher efficiency and power factor than the ITC method with the same operating conditions. Additionally, thermal behaviour of an induction machine fed by a DTC-based FSTP inverter was investigated in [13] where it was concluded that the motor thermal characteristics in the post-fault operating mode are similar to that in the normal operating condition.

The FSTP inverter topology has also been applied to both permanent magnet (PM) brushless DC (BLDC) and brushless AC (BLAC) machines. For the FSTP inverter fed PM BLDC machine drive, a novel current controlled PWM strategy with six commutation modes was proposed [14]. Based on this method, an asymmetrical voltage PWM methodology, together with a sensorless position control strategy utilizing crossing detection of the two active phase voltage waveforms, were proposed to achieve low-cost high-performance [15]. In [16] a DTC-based PM BLDC machine driven by a FSTP inverter that employed novel optimum switching table without requiring explicit stator flux control was proposed. In terms of the PM BLAC machine, a fuzzy logic speed control methodology was developed for an ITC-based FSTP inverter fed interior permanent magnet machine drive [17]. A comparative study in terms of current total harmonic distortion (THD), torque ripple factor (TRF), and performance characteristics between the FSTP and other fault tolerant inverter topologies fed an ITC-based PM BLAC machine drive system was reported in [18]. Simulation study of switching table-based DTC and empirical research of space vector modulation-based DTC applied to a FSTP inverter were conducted in [19] and [20], respectively. However, the phase current waveforms measured under high-speed and load applied conditions in [20] were seriously non-sinusoidal. The authors of a study undertaken in [21] suggested that for a DTC-based FSTP inverter drive system, fast response of torque and flux are top priorities for this control method and not necessarily the reproduction of perfect sinusoidal current waveforms. However, this conclusion appears a little confusing since employing PM BLAC machines dictates the reproduction of sinusoidal current waveforms if the performance of the machine is to be maximized and hence will be one of the issues to be investigated in this paper.

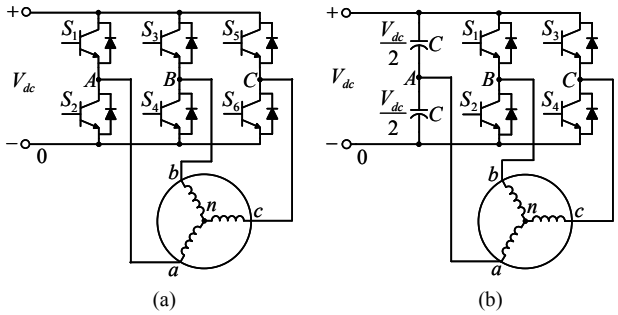

Fig. 1. Inverter topologies. (a) SSTP. (b) FSTP.

In this paper, DTC of a FSTP inverter fed PM BLAC machine is presented and the influence of inverter voltage drop on the performance is investigated and a compensation technique is proposed to mitigate these effects. For control purposes, two stator flux estimation schemes, which are based on current model and voltage model, are respectively discussed. It will be shown that conventional voltage model-based stator flux estimation is inaccurate when used for a FSTP inverter drive system with the DTC methodology owing to neglecting forward voltage of the switching device and its free-wheeling diode which causes an imbalance between the α- and β-flux estimation components if conventional voltage calculation is used. As a result, stator phase current waveforms become significantly distorted and their magnitudes are considerably unbalanced even under high-speed condition and with the presence of a sinusoidal back electromotive-force (emf) PM BLAC machine. To overcome this, a novel voltage compensation scheme for voltage calculation step accounting for the different forward voltage drop values between switching device and free-wheeling diode is proposed and applied in the experimental study. Consequently, the calculation of phase voltages becomes more accurate and therefore voltage model-based DTC methodology becomes much more effective.

TABLE I
VOLTAGE VECTORS OF FSTP INVERTER

$V_{i=1\div4}$	$S_{B,C}$	v_{an}	v_{bn}	v_{cn}	v_{α}	v_{β}
1	00	$V_{dc}/3$	$-V_{dc}/6$	$-V_{dc}/6$	$V_{dc}/3$	0
2	10	0	$V_{dc}/2$	$-V_{dc}/2$	0	$V_{dc}/\sqrt{3}$
3	11	$-V_{dc}/3$	$V_{dc}/6$	$V_{dc}/6$	$-V_{dc}/3$	0
4	01	0	$-V_{dc}/2$	$V_{dc}/2$	0	$-V_{dc}/\sqrt{3}$

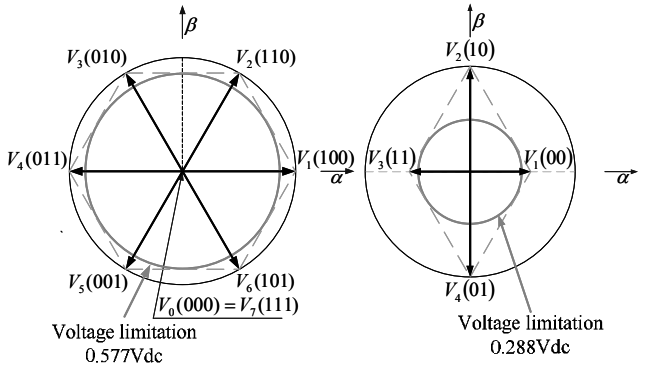

(a) (b)

Fig. 2. Voltage vectors in ($\alpha\beta$) planes. (a) SSTP inverter. (b) FSTP inverter.

II. DTC OF FSTP INVERTER FED PM BLAC MACHINE

A. Mathematical Model of a FSTP Inverter Fed PM BLAC Machine

As mentioned in the introduction, in a FSTP inverter drive system, only two phases of the machine are controlled by power switching devices; the remaining phase is connected directly to the mid-point of DC link via a capacitor divider [4]. This modification reduces the number of power switches from six in a SSTP inverter to four as in a FSTP inverter (Fig. 1). Also from Fig. 1, it can be seen that current balance requirement for a symmetrical three-phase PM BLAC machine can still be satisfied due to the fact that current in phase *A* is contributed by the currents from the two controlled phases *B* and *C*. Additionally, mathematical (*abc*) phase voltage equations describing the SSTP inverter [Fig. 1(a)] can be utilized for the FSTP inverter [Fig. 1(b)] without any modification [6].

$$v_{an} = v_{a0} - v_{n0} = \left(2v_{a0} - v_{b0} - v_{c0}\right)/3 \quad (1)$$

$$v_{bn} = v_{b0} - v_{n0} = \left(2v_{b0} - v_{a0} - v_{c0}\right)/3 \quad (2)$$

$$v_{cn} = v_{c0} - v_{n0} = \left(2v_{c0} - v_{a0} - v_{b0}\right)/3 \quad (3)$$

Since there are only four switches in a FSTP inverter [Fig. 1(b)] the number of switching states is reduced from eight to four with phase-to-zero voltage value of phase *A* held constant at half of DC link voltage value, $V_{dc}/2$. As a result, by way of example, the voltage vectors associated with the switching states of a FSTP inverter, $S_{B,C}$, in which the terminal of phase B or C is connected to the DC link voltage rail if its equivalent switching state is "1" and connected to the zero voltage rail when its equivalent switching state is "0", can be derived as in Table I [6] where their ($\alpha\beta$) components are obtained through applying the Clarke transformation [22] to the (*abc*) phase voltage equations.

$$v_{\alpha} = \left(2v_{an} - v_{bn} - v_{cn}\right)/3 \quad (4)$$

$$v_{\beta} = \left(v_{bn} - v_{cn}\right)/\sqrt{3} \quad (5)$$

The voltage vector information presented in Table I can be employed to obtain the voltage space vectors of a FSTP inverter as represented diagrammatically in Fig. 2(b) [6]. It is worth mentioning that maximum value of the space voltage vector for the low-cost FSTP inverter [Fig. 2(b)] is a half of maximum value of the space voltage vector achievable in a conventional SSTP inverter as illustrated in Fig. 2(a) [5]. Thus, the maximum achievable speed of a machine controlled via a FSTP inverter is half of that achievable with a conventional SSTP inverter.

The well-known mathematical model of a surface-mounted PM BLAC machine in the stationary reference frame ($\alpha\beta$) is the same for both the SSTP and the FSTP inverter topologies [19]-[23].

$$v_{\alpha} = R_s i_{\alpha} + \frac{d}{dt}\psi_{s\alpha} \quad (6)$$

$$v_{\beta} = R_s i_{\beta} + \frac{d}{dt}\psi_{s\beta} \quad (7)$$

$$\psi_{s\alpha} = L_s i_{\alpha} + \psi_m \cos\left(\theta_e\right) \quad (8)$$

$$\psi_{s\beta} = L_s i_{\beta} + \psi_m \sin\left(\theta_e\right) \quad (9)$$

$$T_e = 3p\left(\psi_{s\alpha} i_{\beta} - \psi_{s\beta} i_{\alpha}\right)/2 \quad (10)$$

The magnitude and the angular position of stator flux linkage vector, $|\psi_s|$ and θ_{ψ_s}, are given by

$$|\psi_s| = \sqrt{\psi_{s\alpha}^2 + \psi_{s\beta}^2} \quad (11)$$

$$\theta_{\psi_s} = \arctan\left(\psi_{s\beta}/\psi_{s\alpha}\right) \quad (12)$$

B. Direct Torque Control of a FSTP Inverter Fed PM BLAC Machine

Unlike the ITC technique which employs instantaneous current control [2]-[18], the DTC methodology controls instantaneous torque and flux to achieve high performance operation [1]-[11]. For this purpose, an optimized switching table must be defined based on the output states of the instantaneous stator flux magnitude hysteresis controller and the electromagnetic torque hysteresis controller, together with the equivalent sector in which instantaneous stator flux space vector is located [1]-[11]. Since there are only four available switching states in a FSTP inverter, a modified switching table, in which stator flux ($\alpha\beta$) plane is divided into four different sectors spaced by 90 electrical degrees as shown in Fig. 3, has been introduced in [10]-[19]. The accuracy of both the torque and the flux controllers is based on stator flux linkage, a value which has to be estimated since it cannot be directly measured. Thus, the more accurately the flux can be estimated, the more effective the DTC method is. Normally, flux estimation strategies can be categorized into two main models ─ current model [23], [24] and voltage model [1]-[11], [25], [26], [27].

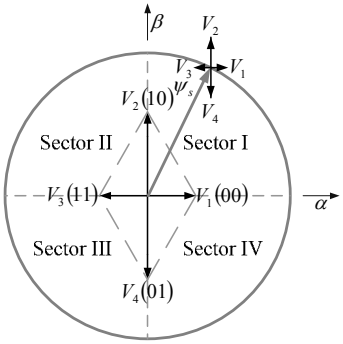

Fig. 3. Control of stator flux linkage with DTC FSTP inverter

TABLE II
SWITCHING TABLE FOR DTC METHOD IN FSTP INVERTER TOPOLOGY

$d\lvert\psi_s\rvert$	dT_e	Sector			
		I	II	III	IV
1	1	$V_2(10)$	$V_3(11)$	$V_4(01)$	$V_1(00)$
	0	$V_1(00)$	$V_2(10)$	$V_3(11)$	$V_4(01)$
0	1	$V_3(11)$	$V_4(01)$	$V_1(00)$	$V_2(10)$
	0	$V_4(01)$	$V_1(00)$	$V_2(10)$	$V_3(11)$

1) Flux estimation by current model

In a current model-based flux estimation scheme, the stator flux is estimated from the measurements of motor currents and rotor position [23], [24]. For current model-based DTC FSTP inverter drive, the stator flux components are predicted by using (8) and (9) [23] and the electromagnetic torque is determined via (10) [1]. Subsequently, magnitude value of the estimated stator flux and the predicted torque value are compared with their reference values, $\lvert\psi_s^*\rvert$ and T_e^*, via two hysteresis comparators to determine equivalent control states (Fig. 4). The outputs of these two hysteresis comparators, $d\lvert\psi_s\rvert$ and dT_e, are determined based on the magnitude stator flux error and the torque error as follows:

$$d\lvert\psi_s\rvert = \begin{cases} 1 & \text{for } \lvert\psi_s^*\rvert - \lvert\psi_s\rvert > \Delta\psi_s/2 \\ 0 & \text{for } \lvert\psi_s^*\rvert - \lvert\psi_s\rvert < -\Delta\psi_s/2 \end{cases} \quad (13)$$

$$dT_e = \begin{cases} 1 & \text{for } T_e^* - T_e > \Delta T_e/2 \\ 0 & \text{for } T_e^* - T_e < -\Delta T_e/2 \end{cases} \quad (14)$$

where $\Delta\psi_s$ is the stator flux hysteresis bandwidth and ΔT_e is the torque hysteresis bandwidth. An optimized lookup table (Table II) is used to translate these two control states, together with the stator flux position information defined in equivalent sector, to the inverter gate drive signals [10]-[12], [19]. This technique has the advantage of not requiring an integration step in the estimation calculation thus removing problems associated with drift and integral windup [25], [26]. However, it does rely on the motor parameters, such as winding inductance and PM flux-linkage, and an expensive position sensor is essential to measure the rotor position.

2) Flux estimation by voltage model

This technique employs the machine voltage equations to estimate the stator flux as follows [1]-[11], [25], [26], [27]:

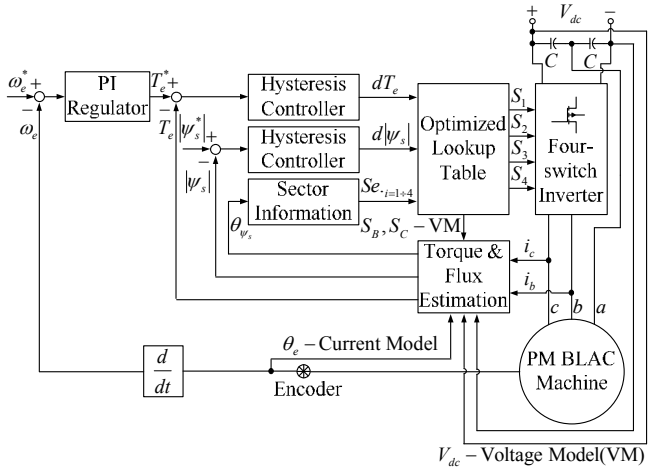

Fig. 4. DTC scheme of PM BLAC machine fed from a FSTP inverter.

$$\psi_{s\alpha} = \int (v_\alpha - R_s i_\alpha) dt \quad (15)$$

$$\psi_{s\beta} = \int (v_\beta - R_s i_\beta) dt \quad (16)$$

The block diagram representation of a FSTP motor drive system regulated by the DTC strategy with voltage model-based flux estimation is the same as that with the current model-based scheme (Fig. 4) where the sensed value of rotor position together with measurements of stator phase currents are used in the current model-based scheme whereas for the voltage model-based scheme knowledge of the instantaneous switching states and measurements of both DC link voltage and motor currents are employed. However, in the voltage model-based flux estimator, an accurate value of winding resistance is required, while the integration step may cause serious problems with unavoidable DC offsets in the measurements of currents and voltages and numerous techniques have been proposed to solve these issues [25], [26], and [27].

In the next section, prediction of stator flux using both the current and voltage model-based schemes will be analyzed, with particular emphasis on the DTC of FSTP inverter fed PM BLAC machine with voltage model-based stator flux estimation.

III. IMBALANCE ISSUES WITH VOLTAGE MODEL-BASED STATOR FLUX ESTIMATION WITH FSTP INVERTER AND IMPROVEMENT

A. Problems of Imbalance with Voltage Model-based Stator Flux Estimation with FSTP Inverter

In a conventional SSTP drive system, two current sensors are used to sense the instantaneous phase currents while the phase voltage values are usually computed directly from the switching states, $S_{A,B,C}$, and the DC link voltage measurement, V_{dc} [11]. For a FSTP drive system, this conventional phase voltage calculation method can be adopted by setting switching state of the stator phase winding connected to midpoint of the DC link (S_A in this paper) to 1/2. Thus,

$$v_{an} = V_{dc}\left(1 - S_B - S_C\right)/3 \quad (17)$$

$$v_{bn} = V_{dc}\left(4S_B - 2S_C - 1\right)/6 \quad (18)$$

$$v_{cn} = V_{dc}\left(4S_C - 2S_B - 1\right)/6 \quad (19)$$

However, in a SSTP inverter, the effects of inverter voltage drop are usually neglected for high-speed operation and some techniques have been proposed for ameliorating these effects at low-speed [28], [29]. In practice, neglecting the inverter voltage drop results in the $\alpha\beta$-stator flux estimator predicts higher values than necessary. Although this does not cause significant problem for stator flux position prediction, it does lead to stator flux magnitude and torque predictions seen by the drive system to be higher than their actual values. As a result, with the same shaft load, the DTC methodology with voltage model-based flux estimator requires increased phase currents compared to actual demand values if voltage drop in switching devices and free-wheeling diodes are not taken into consideration. Despite of these effects, balance is maintained owing to the ballasting effects of the switching device on-state resistances and the forward voltage drops in all three phases in a SSTP drive system, such as that investigated in [29].

On the other hand, in a FSTP inverter, one of the stator phases is directly connected to the DC link mid-point and, thus, the collective balancing effects of inverter on-state resistance and forward voltage drop are lost causing inaccurate stator flux estimation prediction. This phenomenon in a FSTP inverter is explained with reference to a SSTP inverter as follows.

The instantaneous voltage drop of one inverter leg presented by a switching device or a free-wheeling diode, v_{drop}, can be represented by an on-state forward voltage drop, v_f, connected in series with an on-state resistance, R_{on}. Thus,

$$v_{drop} = v_f + iR_{on} \quad (20)$$

Firstly considering just the switching device on-state resistance (i.e. $v_f = 0$), applying (20) to the phase voltage equations [22] leads to,

$$v_{an} = R_s i_a + R_{on} i_a + \frac{d}{dt}\psi_{sa} \quad (21)$$

$$v_{bn} = R_s i_b + R_{on} i_b + \frac{d}{dt}\psi_{sb} \quad (22)$$

$$v_{cn} = R_s i_c + R_{on} i_c + \frac{d}{dt}\psi_{sc} \quad (23)$$

For a SSTP inverter, when transfer to the ($\alpha\beta$) reference frame,

$$\psi_{s\alpha} = \int \left(v_\alpha - R_s i_\alpha - R_{on} i_\alpha\right)dt \quad (24)$$

$$\psi_{s\beta} = \int \left(v_\beta - R_s i_\beta - R_{on} i_\beta\right)dt \quad (25)$$

For a FSTP inverter, phase A is connected to the DC link mid-point and therefore $R_{on} i_a$ does not exist in (21). After transformation this gives,

$$\psi_{s\alpha} = \int \left(v_\alpha - R_s i_\alpha + R_{on} i_\alpha / 3\right)dt \quad (26)$$

$$\psi_{s\beta} = \int \left(v_\beta - R_s i_\beta - R_{on} i_\beta\right)dt \quad (27)$$

TABLE III
FORWARD VOLTAGE DROP ON ONE INVERTER LEG

Switching states	Current direction	v_f
0	+	V_d
	–	$-V_{CE}$
1	+	V_{CE}
	–	$-V_d$

TABLE IV
PARAMETERS OF PROTOTYPE INVERTER DRIVE SYSTEM

V_{CE}	0.9V
V_d	1.25V
R_{on}	0.075Ω

TABLE V
SIMPLE FORWARD VOLTAGE DROP COMPENSATION IN FSTP INVERTER

$sign(i_b)$	$sign(i_c)$	$v_{f\alpha}$	$v_{f\beta}$
–	–	$-2V_f/3$	0
–	+	0	$2V_f/\sqrt{3}$
+	–	0	$-2V_f/\sqrt{3}$
+	+	$2V_f/3$	0

Based on this analysis, the imbalance due to the mid-point phase connection can be clearly seen. The effect of this is for the stator flux α-component to become smaller than the stator flux β-component, with comparison to the conventional SSTP voltage calculation.

Now consider just the inverter forward voltage drop (i.e. $R_{on} = 0$), the phase voltages are given as follows

$$v_{an} = R_s i_a + \frac{d}{dt}\psi_{sa} \quad (28)$$

$$v_{bn} = R_s i_b + v_{fb} + \frac{d}{dt}\psi_{sb} \quad (29)$$

$$v_{cn} = R_s i_c + v_{fc} + \frac{d}{dt}\psi_{sc} \quad (30)$$

where v_{fb} and v_{fc} are the inverter forward voltage drop of phase B and C, respectively. Transforming from the (abc) to the ($\alpha\beta$) reference frames leads to

$$\psi_{s\alpha} = \int \left(v_\alpha - R_s i_\alpha + v_{f\alpha}\right)dt \quad (31)$$

$$\psi_{s\beta} = \int \left(v_\beta - R_s i_\beta + v_{f\beta}\right)dt \quad (32)$$

$$v_{f\alpha} = \left(v_{fb} + v_{fc}\right)/3 \quad (33)$$

$$v_{f\beta} = -\left(v_{fb} - v_{fc}\right)/\sqrt{3} \quad (34)$$

where $v_{f\alpha}$ and $v_{f\beta}$ are the transformed ($\alpha\beta$) inverter forward voltage drop components. According to [30], the inverter forward voltage drop on one inverter leg depends on both its instantaneous switching state and its relevant phase current direction and varies between the values of forward voltage of IGBT, V_{CE}, and its free-wheeling power diode, V_d, as can be seen in Table III.

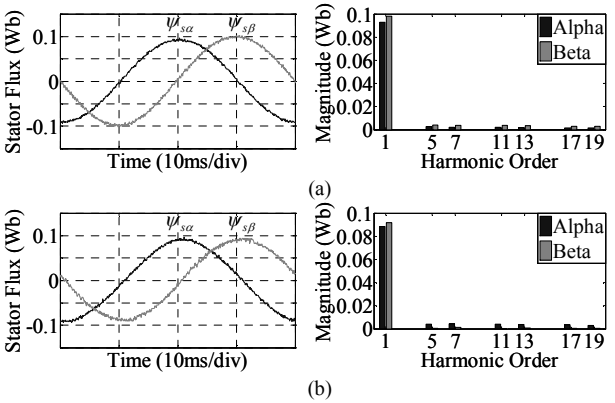

Fig. 5. Experimental results from the voltage model-based stator flux estimation scheme in a FSTP inverter fed PM BLAC machine drive at 1500rpm without compensation for non-ideal switch, full load applied (0.3N.m). (a) Under ITC. (b) Under DTC.

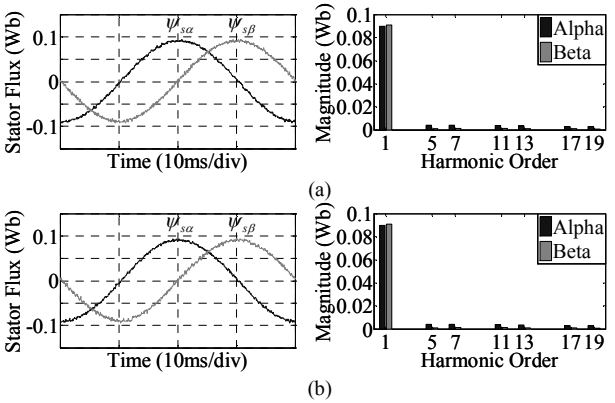

Fig. 6. Experimental results from the voltage model-based stator flux estimation scheme in a FSTP inverter fed PM BLAC machine drive at 1500rpm incorporating the simple voltage drop compensation scheme -Table V, full load applied (0.3N.m). (a) Under ITC. (b) Under DTC.

To simplify the following analysis it is assumed that forward voltages of both switching device and its freewheeling diode have the same value, V_f, and therefore the inverter forward voltage drop depends only on the phase current directions.

$$v_{f\alpha} = V_f\left[sign(i_b) + sign(i_c)\right]/3 \quad (35)$$

$$v_{f\beta} = -V_f\left[sign(i_b) - sign(i_c)\right]/\sqrt{3} \quad (36)$$

Based on the instantaneous phase current directions, the inverter forward voltage drop values in a FSTP inverter can be computed as in Table V. Obviously, unlike the SSTP inverter where the inverter forward voltage drop values are the same in magnitude for α- and β-components as already proven in [29], in a FSTP inverter the β-component of inverter forward voltage drop is higher than that of the α-component, resulting in smaller predicted magnitude of the α-component of stator flux in comparison with that of the β-component.

Finally, combining the effects of both the on-state resistance and the forward voltage drop analyses, it can be concluded that without accounting for the inverter voltage drop, flux estimation values based on the voltage model, (15) and (16), have significantly different α- and β-components. This causes the phase currents measured from the voltage model-based DTC FSTP inverter fed PM BLAC machine drive to exhibit non-sinusoidal waveforms and unbalanced magnitudes due to the incorrect choice of switching states made by the drive system [see Fig. 15 and Fig. 18(a) in Section IV].

TABLE VI
PROPOSED FORWARD VOLTAGE DROP COMPENSATION IN FSTP INVERTER

S_B	S_C	Sign		$v_{f\alpha}$	$v_{f\beta}$
		i_b	i_c		
0	0	−	−	$-2V_{CE}/3$	0
0	1	−	−	$-(V_d+V_{CE})/3$	$-(V_d-V_{CE})/\sqrt{3}$
1	0	−	−	$-(V_d+V_{CE})/3$	$(V_d-V_{CE})/\sqrt{3}$
1	1	−	−	$-2V_d/3$	0
0	0	−	+	$(V_d-V_{CE})/3$	$(V_d+V_{CE})/\sqrt{3}$
0	1	−	+	0	$2V_{CE}/\sqrt{3}$
1	0	−	+	0	$2V_d/\sqrt{3}$
1	1	−	+	$-(V_d-V_{CE})/3$	$(V_d+V_{CE})/\sqrt{3}$
0	0	+	−	$(V_d-V_{CE})/3$	$-(V_d+V_{CE})/\sqrt{3}$
0	1	+	−	0	$-2V_d/\sqrt{3}$
1	0	+	−	0	$-2V_{CE}/\sqrt{3}$
1	1	+	−	$-(V_d-V_{CE})/3$	$-(V_d+V_{CE})/\sqrt{3}$
0	0	+	+	$2V_d/3$	0
0	1	+	+	$(V_d+V_{CE})/3$	$-(V_d-V_{CE})/\sqrt{3}$
1	0	+	+	$(V_d+V_{CE})/3$	$(V_d-V_{CE})/\sqrt{3}$
1	1	+	+	$2V_{CE}/3$	0

In order to further highlight the aforementioned problem, the estimated stator fluxes under both ITC [18] and DTC are presented in Fig. 5. As can be seen from Fig. 5(a), the α- and β-components of stator flux, both magnitudes and harmonics, are clearly different under ITC. However, under DTC, although the peaks of α- and β-components of stator flux are directly controlled and forced to be equal, the magnitudes of the fundamental and high-order harmonics are still different [see Fig. 5(b)].

B. Compensation of Inverter Voltage Drop in Voltage Model-based Stator Flux Estimation with FSTP Inverter

Compensation for inverter forward voltage drop in a SSTP inverter drive system to improve its low-speed operation was proposed for an induction machine sensorless drive [28] and a DTC-based interior permanent magnet machine drive [29] by adding appropriate voltage values to the machine voltage equations with assumption that forward voltage drop of switching device and freewheeling power diode are equal. Although this hypothesis can be accepted for the SSTP inverter topology with similar voltage drop values present in all stator phases, a more accurate voltage compensation table should be defined for the FSTP inverter topology because serious problems of unbalanced magnitude and non-sinusoidal current waveforms caused by the asymmetric inverter voltage drop cannot be effectively handled by the simple forward voltage drop compensation presented in Table V. As can be

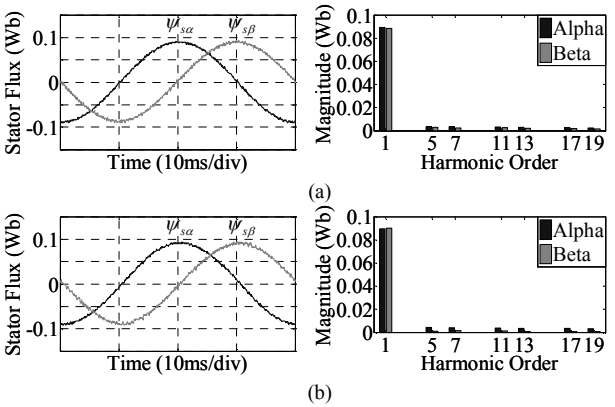

Fig. 7. Experimental results from the voltage model-based stator flux estimation scheme in a FSTP inverter fed PM BLAC machine drive at 1500rpm incorporating the proposed voltage drop compensation scheme - Table VI, full load applied (0.3N.m). (a) Under ITC. (b). Under DTC.

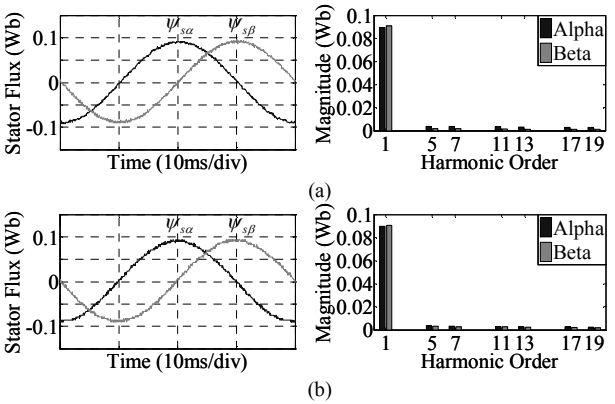

Fig. 8. Experimental results from the current model-based stator flux estimation scheme in a FSTP inverter fed PM BLAC machine drive at 1500rpm, full load applied (0.3N.m). (a) Under ITC. (b) Under DTC.

seen from Fig. 6, the magnitudes of the fundamental and the high-order harmonics of predicted stator flux waveforms estimated by a voltage model-based stator flux estimator incorporating this simple forward voltage drop compensation scheme, $V_f = 0.9V$, still exhibit considerable difference between the α- and β-components for both the ITC-based and DTC-based FSTP drive systems. Table VI shows the proposed compensation forward voltage drop $v_{f\alpha}$ and $v_{f\beta}$ derived from (33), (34), and Table III which are to be added to the flux equations in the ($\alpha\beta$) reference frame according to the switching states and phase current directions. Voltage compensation strategies applied to flux equations are outlined below with reference to Table V for the simple scheme and Table VI for the proposed scheme.

$$\psi_{s\alpha} = \int \left(v_\alpha - R_s i_\alpha + v_{f\alpha} + R_{on} i_\alpha / 3\right) dt \quad (37)$$

$$\psi_{s\beta} = \int \left(v_\beta - R_s i_\beta + v_{f\beta} - R_{on} i_\beta\right) dt \quad (38)$$

Fig. 7 shows the predicted stator flux waveforms for both the ITC-based and DTC-based FSTP drive systems employing a voltage model-based estimator incorporating the proposed voltage drop compensation scheme for the prototype FSTP inverter. As can be seen, the imbalance between α- and β-flux components is significantly reduced.

C. Current Model-based Stator Flux Estimation with FSTP Inverter

The current model-based stator flux estimation can be considered as an alternative method to avoid the aforementioned imbalanced inverter voltage drop amongst three phases in a FSTP inverter. Fig. 8 shows the corresponding measured stator flux waveforms under both the ITC and DTC methods where natural balance between the α- and β-flux components can be obviously recognized.

IV. Experimental Results

In this section the measured DTC performance of a prototype FSTP inverter with the current model-based and the voltage model-based stator flux estimation is presented. The drive system is controlled by a 32-bit fixed-point TMS320-F2812 DSP. It has an inner loop sample time of 50μs for torque and flux control and the outer speed control loop is set to 10 times slower. The phase currents are measured by two closed-loop Hall-effect current sensors while the DC link voltage is measured by a closed-loop Hall-effect voltage sensor. In addition, for the voltage model-based stator flux estimation scheme, the terminal phase voltages are computed from both the measured DC link voltage and the switching states of the inverter and a low-pass filter with a cut-off frequency of 5(rad/s) is utilized instead of a pure integrator to avoid integration drift problems [27]. For simplicity, ΔT_e and $\Delta\psi_s$ is set to zero. Pictures of the experimental setup are shown in Fig. 9. The machine employed has sinusoidal but slightly unbalanced back-emf values [see Fig. 9(c) and Table VII] and their effects on machine operation were discussed in detail in [31]. Parameters of the tested machine are presented in Table VIII and more details can be found in [31] and [32]. A brushed DC generator is used to apply different load torque conditions. The full load applied to the PM BLAC machine is its rated torque (0.3N.m) of which magnitude value of current demand is 2.2A. The stator flux linkage reference, $|\psi_s^*|$, is set to peak value of the PM flux-linkage (92.8mWb). In terms of inverter design, an International Rectifier's IRAMY20UP60B intelligent power module (IPM) with boot-strap technique dedicated for appliance motor drive applications was chosen to expedite development. For each test the machine was run at 1500 rpm (half of its rated speed) for one hour period with half load applied in the first half hour period and full load applied in the second half hour period. During each test, every 5 minutes, an infrared thermometer (Raytek Raynger ST60) was used to sense case temperature of the IPM as shown in Fig. 10 while the room temperature was kept around 21°C and the IPM was mounted on a heatsink and naturally cooled [Fig. 9(a)]. To elucidate the influence of the unbalanced inverter leg voltage drops and the effect of the two aforementioned compensation schemes in a DTC-based FSTP inverter, stator phase currents and electromagnetic torque were measured at the beginning of the test duration with inertial load applied (25% of full load) and at the end of every half hour period

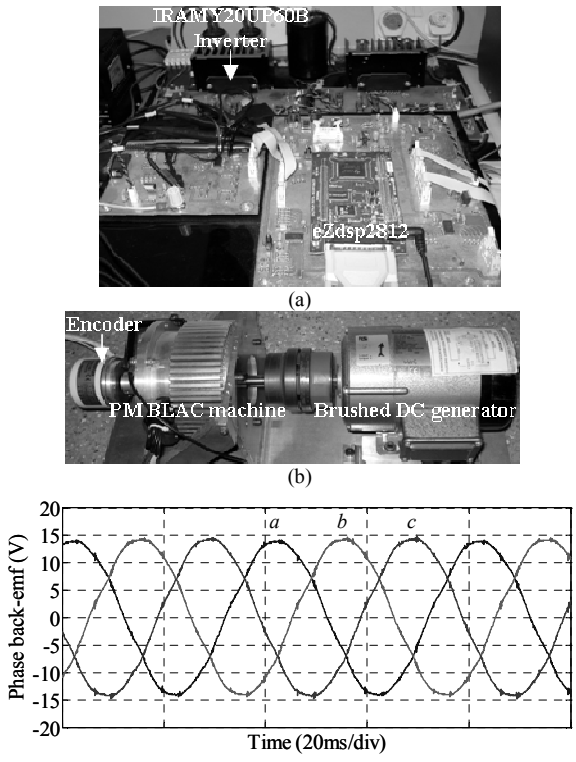

Fig. 9. Experimental test-rig. (a) FSTP inverter and DSP control unit. (b) PM BLAC machine couple with brushed DC generator and incremental encoder (2000pulse/rev). (c) Measured back-emf waveforms of the prototype machine at 1500rpm.

TABLE VII
PHASE BACK-EMF HARMONICS (V) AT 1500RPM

Phase	A	B	C
Fundamental	14.0868	14.2880	14.4254
3rd	0.0488	0.0321	0.0364
5th	0.2385	0.2483	0.2209
7th	0.2274	0.2375	0.2472

TABLE VIII
PARAMETERS OF PROTOTYPE PM BLAC MACHINE

Phase resistance	0.466 Ω
Dq-axis inductance	3.19 mH
PM flux-linkage	92.8 mWb
Number of pole pairs	1
DC bus voltage	70 V
Rated speed	3000 rpm
Rated torque	0.3 N.m
Rated current	2.2 A

when case temperature of the IPM reached to the steady state (see Fig. 10). To demonstrate the performance of the FSTP inverter topology, operation of the machine driven by a conventional SSTP inverter is undertaken first and total harmonic distortion (THD) of phase currents and torque ripple factor (TRF) in every test with full load applied (0.3N.m) are analysed and presented (Table X). Definitions of these factors are given by

$$THD_X = \frac{\sqrt{\sum_{n=2}^{\infty} X_n^2}}{X_1} 100\% \; ; \; THD = \sqrt{\frac{THD_A^2 + THD_B^2 + THD_C^2}{3}} \quad (39)$$

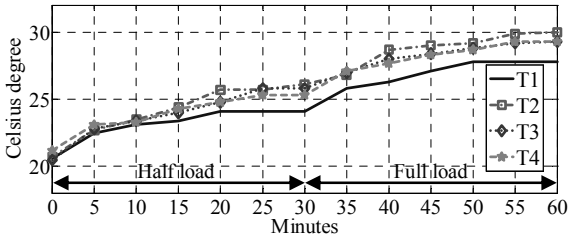

Fig. 10. Temperature measurements of the IPM case for each test of the FSTP inverter. T1 is for current model-based DTC. T2 is for voltage model-based DTC without compensation. T3 and T4 are for voltage model-based DTC with the compensation scheme in Table V and Table VI, respectively.

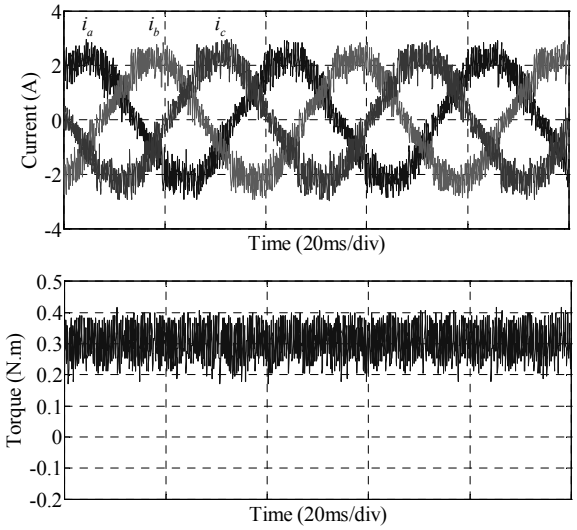

Fig. 11. Measured results from the current model-based DTC SSTP inverter at 1500rpm, full load applied (0.3N.m).

where X_1 is the fundamental harmonic, X_n is the high-order harmonic, THD_X is the harmonic distortion factor of one stator phase, and THD is the total harmonic distortion factor.

$$TRF = \frac{T_{m,pk-pk}}{T_{rated}} \cdot 100\% \quad (40)$$

where T_{rated} is the rated torque and $T_{m,pk-pk}$ is the measured peak-to-peak torque ripple value.

Comparison of the current and torque results for the current model-based DTC FSTP inverter [Fig. 12 (c)] with similar results derived from the SSTP inverter (Fig. 11) shows that a similar performance can be obtained using a simpler drive topology. However, because phase A terminal in the FSTP inverter is connected directly to the DC link mid-point, the current waveform of phase A only contains switching ripple contributed from the two active-phase currents. Hence, as can be seen in Table IX and Table X, both fundamental phase current values, phase current THD value, and TRF value of the machine driven by a FSTP inverter are lower than that in a SSTP inverter driven case under the same operating conditions. Additionally, based on sinusoidal current waveforms measured under various torque conditions as shown in Fig. 12, it can be proven that the current model-based DTC FSTP scheme is completely not affected by the aforementioned imbalanced issue in the inverter voltage drop.

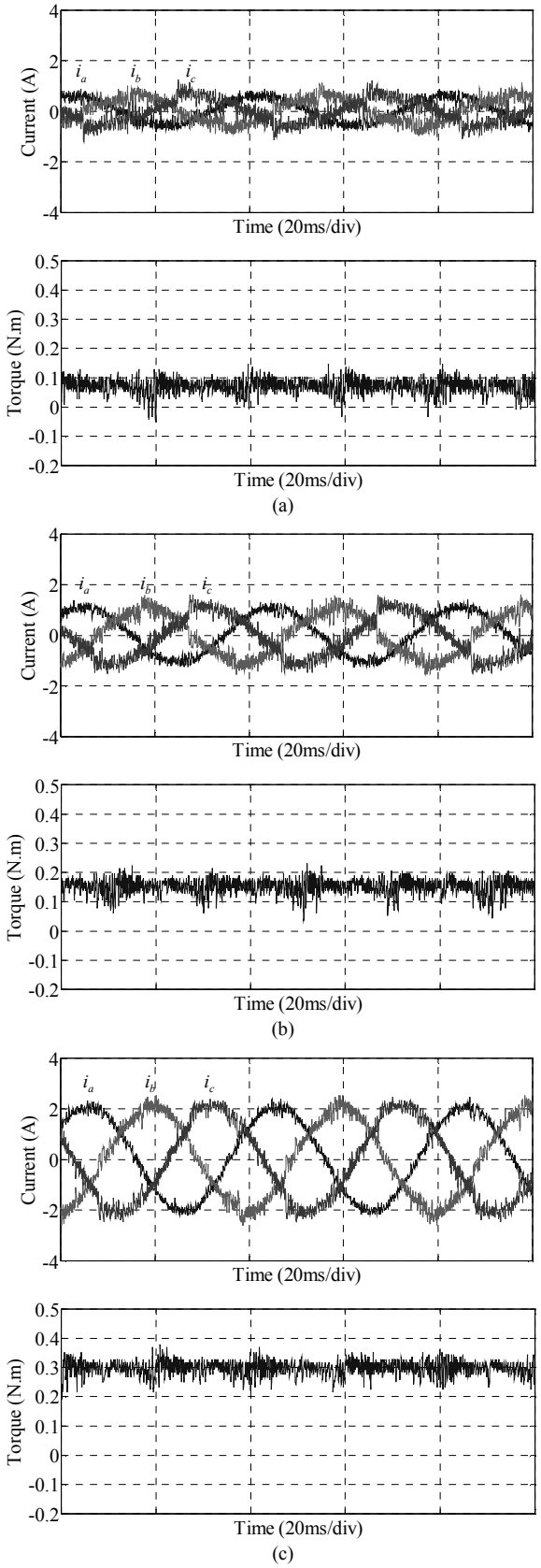

Fig. 12. Measured results under various torque conditions from the current model-based DTC FSTP inverter at 1500rpm. (a) Inertial load. (b) Half load. (c) Full load (0.3N.m).

The following sets of results (Figs. 13-20) are for voltage model-based DTC control. It is worth noting that the back-emf values of the tested PM BLAC machine slightly vary phase to phase as shown in Table VII and, although this problem does not affect torque response inadvertently, it does make the fundamental current waveforms slightly unbalanced (Table IX). Therefore, simulation results are presented in Fig. 14 to clearly demonstrate this effect.

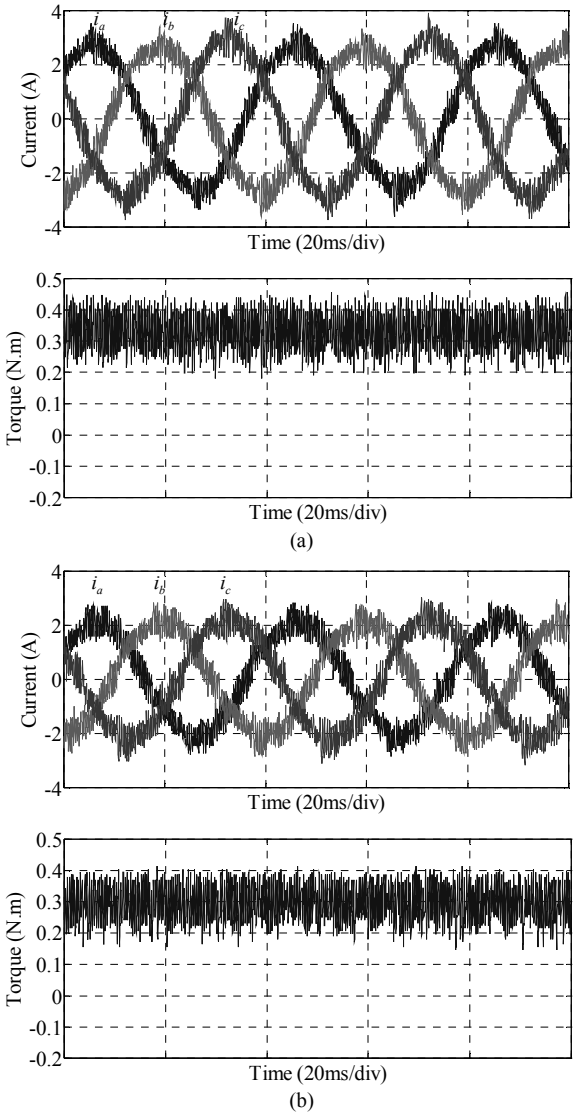

Fig. 13. Measured results from the voltage model-based DTC SSTP inverter at 1500rpm, full load applied (0.3N.m). (a) Without voltage drop compensation. (b) With voltage drop compensation [29].

Fig. 13 shows the experimental results of the voltage model-based flux estimation DTC SSTP drive system without and with including the voltage drop compensation outlined in [29]. It is obvious that current waveforms in this topology are non-ideal since the motor back-emf waveforms differ in peak value and exhibit pole pulsation. Similarly, since (10) is used to estimate the torque, prediction errors from the flux estimator can propagate through the current controller. Thus, in the absence of inverter leg voltage drop compensation, the estimated torque value seen by the drive system is higher than the actual demanded shaft torque value of 0.3N.m (Table X);

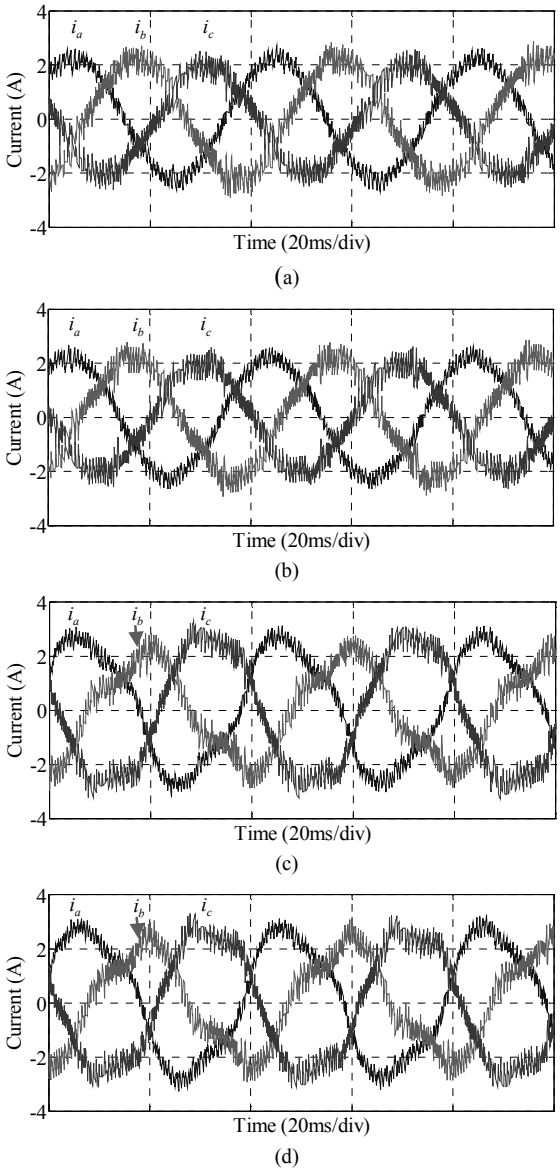

Fig. 14. Simulated currents from the voltage model-based DTC FSTP inverter at 1500rpm without inverter voltage drop compensation, full load applied (0.3N.m). (a) Balanced back-emfs and ideal switches. (b) Unbalanced back-emfs and ideal switches. (c) Balanced back-emfs and non-ideal switches. (d) Unbalanced back-emfs and non-ideal switches.

in turn this causes the controller to force the phase currents to be higher than the actual demand values (2.2A) in order to satisfy this incorrectly estimated torque value (Table IX). However, current waveforms are still sinusoidal because the inverter voltage drop is balanced between α- and β-components in a SSTP inverter drive system [29]. Under compensation scheme with the assumption that the value of forward voltage drop in switching device and free-wheeling diode are the same [29], performance of the drive system was improved [see Fig. 13(b), Table IX and Table X].

To further examine the effects of inverter voltage drop and back-emf non idealities on the phase current waveform distortion, in Fig. 14, a simulation investigation utilizing MATLAB/SIMULINK was performed to act as a benchmark

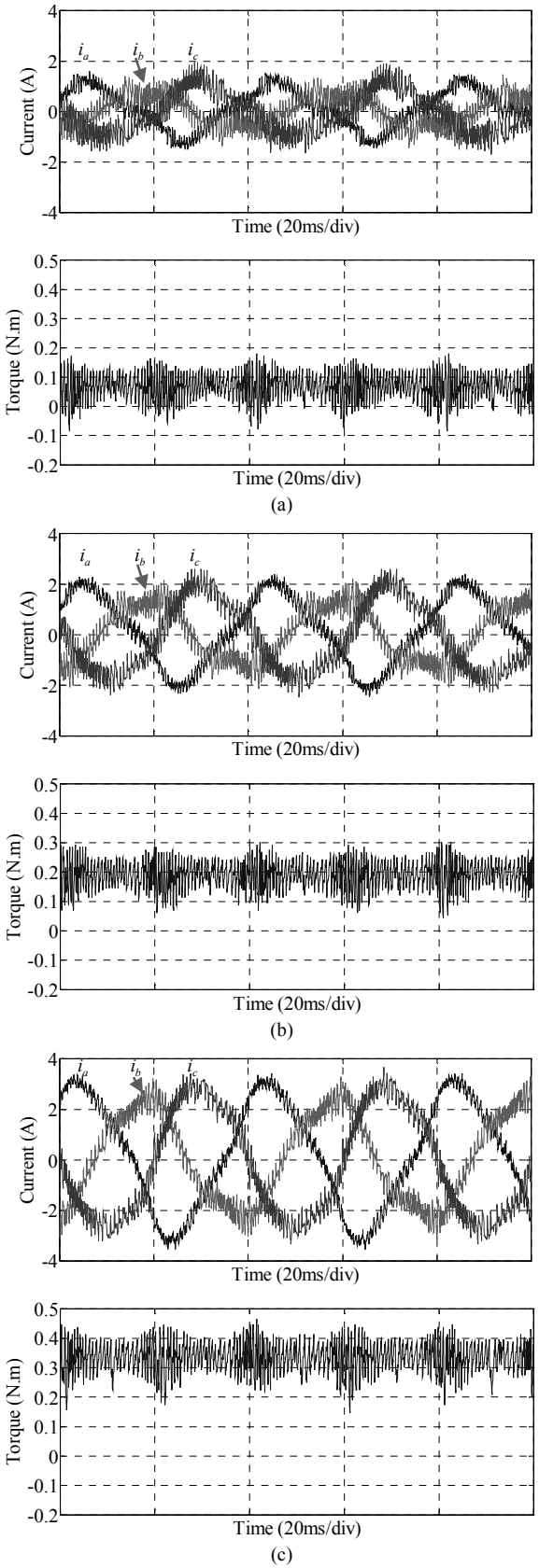

Fig. 15. Measured results under various torque conditions from the voltage model-based DTC FSTP inverter at 1500rpm without compensation for non-ideal switch. (a) Inertial load. (b) Half load. (c) Full load (0.3N.m).

TABLE IX
FUNDAMENTAL VALUES OF PHASE CURRENTS (A) UNDER VARIOUS CONTROL SCHEMES BUT THE SAME SPEED (1500RPM) AND FULL TORQUE (0.3N.M) OPERATING CONDITIONS

Topology	Phase A	Phase B	Phase C
Current model-based DTC			
SSTP	2.22	2.20	2.29
FSTP	2.05	2.06	2.12
Voltage model-based DTC-without compensation			
SSTP	2.74	2.73	2.89
FSTP	2.97	2.37	3.00
Voltage model-based DTC-with compensation			
SSTP [29]	2.13	2.13	2.25
Simple-FSTP	2.53	2.37	2. 41
Proposed-FSTP	2.26	2.16	2.16

TABLE X
CALCULATION OF DC-COMPONENT OF PREDICTED TORQUE (N.M) , CURRENT THD, AND TRF OF DTC SSTP AND FSTP SCHEMES AT 1500RPM AND FULL TORQUE (0.3N.M) OPERATING CONDITIONS

	Predicted torque	$THD(\%)$	$TRF(\%)$
Current model-based DTC			
SSTP	0.3034	7.84	86.27
FSTP	0.2973	7.40	60.39
Voltage model-based DTC without compensation			
SSTP	0.3296	7.70	92.02
FSTP	0.3345	7.20	92.02
Voltage model-based DTC with compensation			
SSTP [29]	0.2984	8.99	89.15
Simple-FSTP	0.3046	8.83	89.15
Proposed-FSTP	0.2989	7.16	86.27

for the inverter voltage drop compensation results. Fig. 14(a) shows sinusoidal current waveforms derived from the simulation model implemented with balanced back-emfs (Table VIII) and ideal switching devices where the values of inverter on-state resistance and on-state forward voltage drop are set to zero. These current waveforms became unbalanced in magnitude when measured values for unbalanced back-emfs of the tested machine (Table VII) were applied to the simulation model [Fig. 14(b)]. Fig. 14(c) also shows current waveform distortion with the non-ideal switching devices applied in isolation (Table IV). The current distortion is more severe when the real unbalanced back-emfs were employed together with the non-ideal switching devices in the simulation model [Fig. 14(d)]. Fig. 15 presents the measured currents under various torque conditions from the voltage model-based flux estimation DTC FSTP inverter without inverter voltage drop compensation. Because of the imbalance in α- and β-stator flux components when they are estimated by the conventional method neglecting the inverter voltage drop, the instantaneous estimated values of stator flux magnitude and electromagnetic torque become incorrect and cause the DTC drive system to make wrong decision when choosing appropriate switching states. Hence, the current waveforms become very non-sinusoidal and unbalanced in magnitude even when the machine was driven under the maximum achievable speed and rated torque conditions [Fig. 15 (c) and Table IX] (similar phenomena can be found in [20] and [31]). Additionally, it can be seen in Fig. 15(c) that by neglecting inverter non-idealises, the torque estimation accuracy is also compromised with the estimated torque seen by the drive system is higher than the actual torque value (0.3N.m) (Table X). In practice, the higher torque prediction with higher current demand under the same speed and torque conditions will limit the maximum achievable motor torque.

The improvements in balanced magnitude values and waveform shapes of the phase currents under various torque conditions achieved by including the proposed forward voltage drop compensation scheme (Table VI) in the flux estimator can clearly be seen by comparing Fig. 15 with Fig. 17. Incorporating this proposed compensation scheme, the current waveforms achieve satisfactory sinusoidal shapes and balanced magnitude values even under inertial torque condition [Fig. 17(a)] and half torque condition [Fig. 17(b)]. The proposed voltage compensation scheme also reduced the torque calculation offset (Fig. 17 and Table X) and therefore also reduced stator phase current magnitude values (Table IX).

Comparing the proposed inverter voltage drop compensation scheme (Table VI) and the simple inverter voltage drop compensation scheme (Table V) it is obvious from Table IX and Table X that the simple forward voltage drop compensation scheme with the assumption that the voltage drop of switching device and free-wheeling diode has the same value is not adequate enough to compensate for the predicted stator flux imbalance in a voltage model-based DTC FSTP inverter fed PM BLAC machine drive. Although the enhancement of the phase current waveforms and the reduction of torque error offset can be observed in Fig. 16 and Table X, its fundamental current values are still higher than the actual demand value (2.2A) under the same speed and full load applied (0.3N.m) conditions (Table IX). Besides, neither phase current THD value nor TRF value of the drive system under this simple compensation scheme does achieve significant improvement in comparison with performance of the SSTP inverter included inverter voltage drop compensation [29] under the same operating conditions (Table X). On the other hand, when adapting the proposed voltage drop compensation scheme in Table VI to the voltage model-based DTC FSTP inverter under the same operating conditions, it can be seen that not only high improvement in the current waveforms can be achieved (Fig. 17) but also current THD value and TRF value become lower than that of a SSTP inverter (Table X).

For completeness current waveforms taken from the motor operating at lower speeds are presented in Figs. 18-20 to demonstrate the improvement gained using the proposed inverter voltage drop compensation scheme (Table VI) in comparison with the simple scheme (Table V). In Fig. 18 current waveforms with the motor operating at 700rpm are presented clearly showing the improvement achievable using the voltage-drop compensation scheme. Additionally, by comparing Fig. 18(c) to Fig. 18(b), it can be clearly seen that performance of the voltage model-based DTC FSTP inverter with the proposed inverter voltage drop compensation scheme (Table VI) achieves lower phase current magnitudes than that

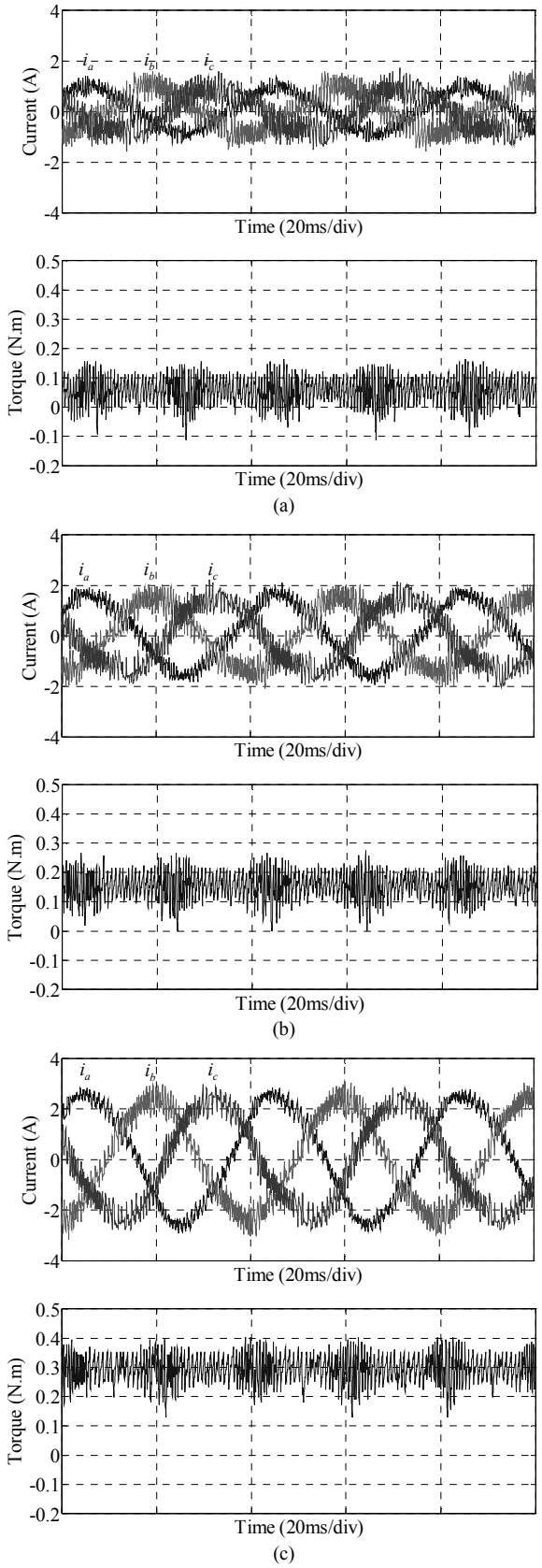

Fig. 16. Measured results under various torque conditions from the voltage model-based DTC FSTP inverter at 1500rpm incorporating the simple voltage drop compensation scheme - Table V. (a) Inertial load. (b) Half load. (c) Full load (0.3N.m).

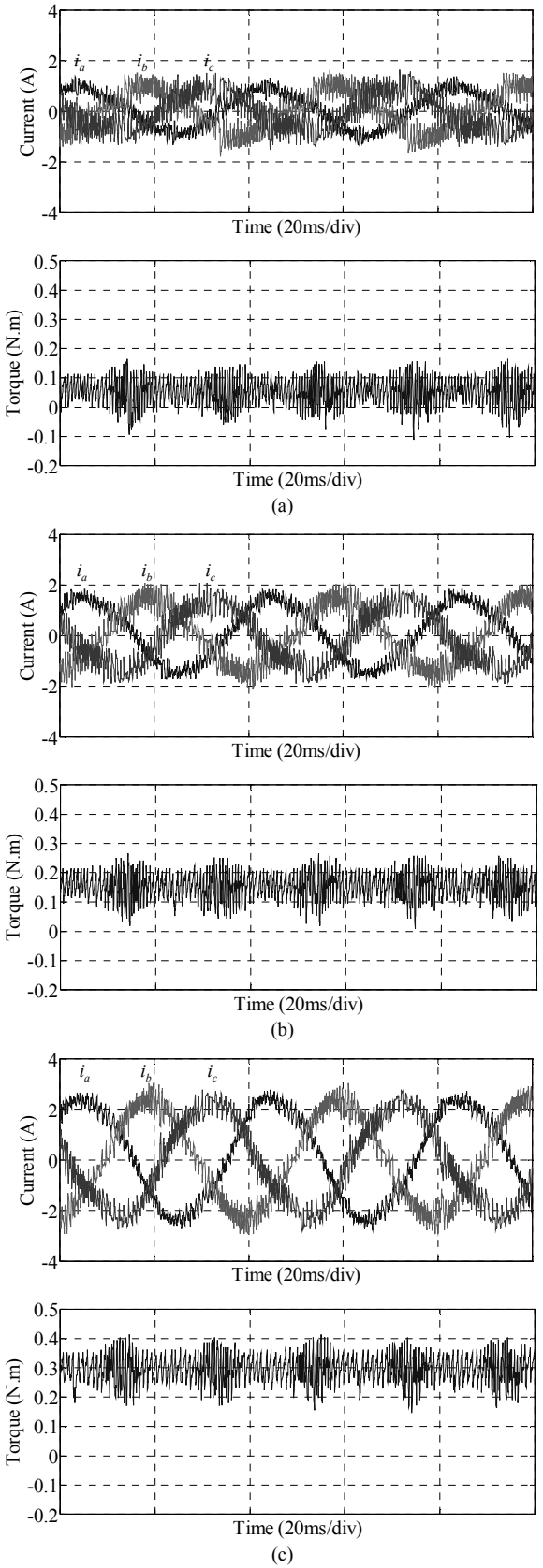

Fig. 17. Measured results under various torque conditions from the voltage model-based DTC FSTP inverter at 1500rpm incorporating the proposed voltage drop compensation scheme - Table VI. (a) Inertial load. (b) Half load. (c) Full load (0.3N.m).

with the simple inverter voltage drop compensation scheme

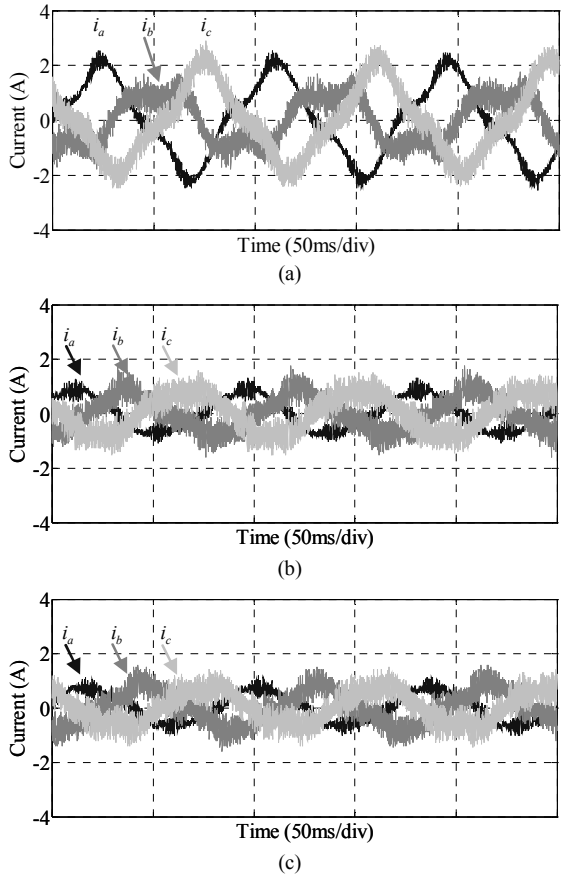

Fig. 18 Measured results of the voltage model-based DTC FSTP inverter at 700rpm with inertial load. (a) Without compensation for non-ideal switch. (b) Incorporating the simple compensation scheme - Table V. (c) Incorporating the proposed compensation scheme - Table VI.

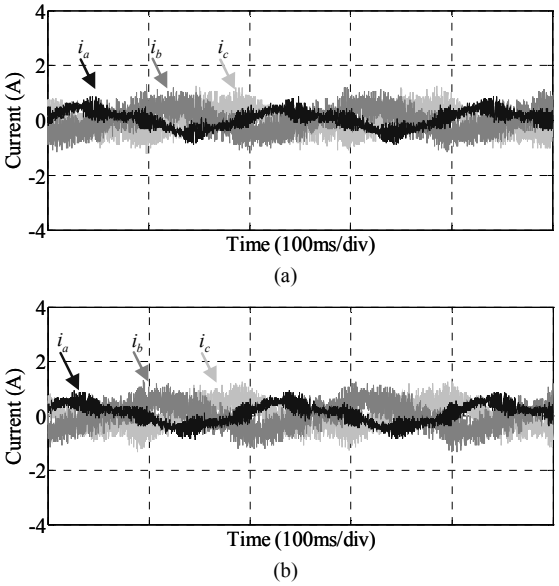

Fig. 19. Measured results of the voltage model-based DTC FSTP inverter at 300rpm with inertial load. (a) Incorporating the simple compensation scheme - Table V. (b) Incorporating the proposed compensation scheme - Table VI.

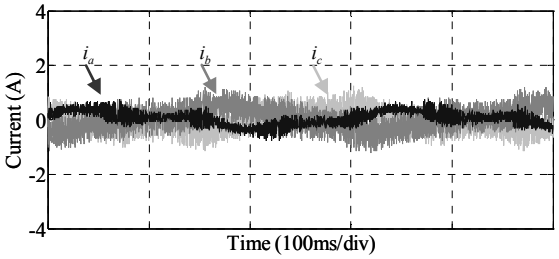

Fig. 20. Measured results of the voltage model-based DTC FSTP inverter at 200rpm incorporating the proposed compensation scheme - Table VI, initial load.

(Table V) under the same torque condition. Since the drive system without inverter voltage drop compensation cannot be readily operated at the speed condition lower than 700rpm due to the serious phase current distortion, only current waveform measurements of the drive system featuring inverter voltage drop compensation at 300rpm are shown in Fig. 19. Fig. 20 presents current waveforms measured at 200rpm of the drive system incorporating the proposed inverter voltage drop compensation scheme.

V. CONCLUSIONS

This paper has presented DTC of FSTP inverter fed a PM BLAC machine, investigated the influence of inverter voltage drop on the performance and proposed its compensation technique. Both the current model-based and the voltage model-based stator flux estimation schemes are discussed, with reference to a SSTP inverter.

It has been found that when derived from the conventional voltage model-based stator flux estimation scheme, the predicted stator flux imbalance may be caused by the unbalanced inverter voltage drop in the FSTP inverter topology in which one phase winding is directly connected to the DC link mid-point. Whilst this imbalanced predicted stator flux problem does not exist and affect the performance of current model-based DTC, it causes significant non-sinusoidal current waveforms and considerable unbalanced current magnitudes in the voltage model-based DTC. It is also proven that for a FSTP inverter, the simple inverter voltage drop compensation scheme with the assumption that the voltage drop value of switching device and free-wheeling diode are the same is not adequate enough. Therefore, a new inverter voltage drop compensation scheme accounting for the different voltage drop values for the switching device and the free-wheeling diode has been proposed for the voltage-based DTC to correct for the predicted stator flux imbalance. This was achieved via the addition of corrective voltages to the flux equations to represent these voltage drops. The proposed scheme has improved the shape of current waveforms and resulted in satisfactory balanced current magnitudes as verified by both the simulation and experimental results (corresponding simulation results confirm those measured results although only selected simulated results are given in the paper due to space limit).

It has been shown that it is possible for a low cost or post fault-tolerant FSTP inverter to provide similar performance to a SSTP inverter when driving a PM BLAC machine. Analysis of the phase current THD and TRF showed that the FSTP

inverter presented lower harmonic distortion and torque ripple than the conventional SSTP inverter when these drive systems were operated under the same speed and torque conditions.

REFERENCES

[1] L. Zhong, M. F. Rahman, W. Y. Hu, and K. W. Lim, " Analysis of direct torque control in permanent magnet synchronous motor drives," *IEEE Trans. Power Electron.*, vol. 12, no. 3, pp. 528–536, May 1997.

[2] P. Pillay and R. Krishnan, "Modelling, simulation, and analysis of permanent-magnet motor drives, part I: the permanent-magnet synchronous motor drive," *IEEE Trans. Ind. Appl.*, vol. 25, no. 2, pp. 265–273, Mar./Apr. 1989.

[3] B. A. Welchko and T. A. Lipo, "A novel variable-frequency three-phase induction motor drive system using only three controlled switches," *IEEE Trans. Ind. Appl.*, vol. 32, no. 6, pp. 1739–1745, Nov./Dec. 2001.

[4] H. W. van der Broeck and J. D. van Wyk, "A comparative investigation of a three-phase induction machine drive with a component minimized voltage-fed inverter under different control options," *IEEE Trans. Ind. Appl.*, vol. IA-20, no. 2, pp. 309–320, Mar./Apr. 1984.

[5] B. A. Welchko, T. A. Lipo, T. M. Jahns, and S. E. Schulz, "Fault tolerant three-phase AC motor drive topologies: a comparison of features, cost, and limitations" *IEEE Trans. Power Electron.*, vol. 19, no. 4, pp. 1108–1116, Jul. 2004.

[6] F. Blaabjerg, S. Freysson, H. H. Hansen, and S. Hansen, "A new optimized space-vector modulation strategy for a component-minimized voltage source inverter," *IEEE Trans. Power Electron.*, vol. 12, no. 4, pp. 704–714, Jul. 1997.

[7] M. B. R. Corrêa, C. B. Jacobina, E. R. C. da Silva, and A. M. N. Lima, "A general PWM strategy for four-switch three-phase inverters," *IEEE Trans. Power Electron.*, vol. 21, no. 6, pp. 1618–1627, Nov. 2006.

[8] J. Kim, J. Hong, and K. Nam, "A current distortion compensation scheme for four-switch converters," *IEEE Trans. Power Electrons.*, vol. 24, no. 4, pp. 1032–1040, Apr. 2009.

[9] J.-R. Fu and T. Lipo, "A strategy to isolate the switching device fault of a current regulated motor drive," in *Conf. Rec. IEEE − IAS Annu. Meeting*, 1993, vol. 01, pp. 1015–1020.

[10] M. Azab and A. L. Orille, "Novel flux and torque control of induction motor drive using four switch three phase inverter," in *Proc. IEEE Annu. Conf. Ind. Electron. Soc.*, 2001, vol. 2, pp. 1268–1273.

[11] I. Takahashi and T. Noguchi, "A new quick-response and high-efficiency control strategy of an induction motor," *IEEE Trans. Ind. Appl.*, vol. IA-22, no. 5, pp. 820–827, Sept./Oct. 1986.

[12] A. M. S. Mendes and A. J. M. Cardoso, "Fault-tolerant operating strategies applied to three-phase induction-motor drives," *IEEE Trans. Ind. Electron.*, vol. 53, no. 6, pp. 1807–1817, Dec. 2006.

[13] A. M. S. Mendes, X. M. Lopez-Fernandez, and A. J. M. Cardoso, "Thermal performance of a three-phase induction motor under fault tolerant operating strategy," *IEEE Trans. Power Electron.*, vol. 23, no. 3, pp. 1537–1544, May 2008.

[14] B.-K. Lee, T.-H. Kim, and M. Ehsani, "On the feasibility of four-switch three-phase BLDC motor drives for low cost commercial application: Topology and control," *IEEE Trans. Power Electron.*, vol. 18, no. 1, pp. 164–172, Jan. 2003.

[15] C.-T. Lin, C.-W. Hung, and C.-W. Liu, "Position sensorless control for four-switch three-phase brushless DC motor drives," *IEEE Trans. Power Electron.*, vol. 23, no. 1, pp. 438–444, Jan. 2008.

[16] S. B. Ozturk, W. C. Alexander, and H. A. Toliyat, "Direct torque control of four-switch brushless DC motor with non-sinusoidal back EMF," *IEEE Trans. Power Electron.*, vol. 25, no. 2, pp. 263–271, Feb. 2010.

[17] M. N. Uddin, T. S. Radwan, and M. A. Rahman, "Fuzzy-logic-controller-based cost-effective four-switch three-phase inverter-fed IPM synchronous motor drive system," *IEEE Trans. Ind. Appl.*, vol. 42, no. 1, pp. 21–30, Jan./Feb. 2006.

[18] K. D. Hoang, Z. Q. Zhu, M. P. Foster, and D. A. Stone, "Comparative study of current vector control performance of alternate fault tolerant inverter topologies for three-phase PM brushless AC machine with one phase open-circuit fault," *International Conference on Power Electronics, Machine and Drives*, Brighton, April 19–21, 2010, paper Mo4.1.3.

[19] D. Sun and J. Meng, "Research on fault tolerant inverter based permanent magnet synchronous motor direct torque control drives," in *Proc. IEEE Int. Conf. Ind. Electron. Appl.*, Singapore, May 24–26, 2006, pp. 1–5.

[20] D. Sun, Z. He, Y. He, and Y. Guan, "Four-switch inverter fed PMSM DTC with SVM approach for fault tolerant operation," in *Proc. IEEE Int. Conf. Electrical Machines and Drives*, May 3–5, 2007, vol. 1, pp. 295–299.

[21] D. Sun, X. Liu, L. Shang, and Y. B. Ivonne, "Four-switch three-phase inverter fed DTC system considering DC-link voltage imbalance," in *Proc. IEEE Int. Conf. Electrical Machines and Systems*, Oct. 17–20, 2008, pp. 1068–1072.

[22] P. C. Krause, O. Wasynczuk, and S. D. Sudhoff, *Analysis of electric machinery and drive systems*, *2nd* ed., New York: Wiley-IEEE Press, 2002, ch. 4 and ch. 6.

[23] J. Mengjia, S. Cenwei, Q. Jianqi, and L. Ruiguang, "Stator flux estimation for direct torque controlled surface mounted permanent magnet synchronous motor drives over wide speed region," *Proceedings of the Eighth International Conference on Electrical Machines and Systems*, 27–29 Sept. 2005, vol. 1, pp. 350–354.

[24] V. Kremer, Z. Q. Zhu, and D. Howe, "Indirect and direct force control of a two-phase tubular permanent magnet machine," *IEEE Trans. Power Electron.*, vol. 22, no. 2, pp. 654–662, Mar. 2007.

[25] J. Hu, and B. Wu, "New integration algorithms for estimating motor flux over a wide-speed range," *IEEE Trans. Power Electron.*, vol. 13, no. 5, pp. 969–977, Sep. 1998.

[26] M. F. Rahman, Md. E. Haque, L. Tang, and L. Zhong, "Problems associated with the direct torque control of an interior permanent-magnet synchronous motor drive and their remedies," *IEEE Trans. Ind. Electron.,* vol. 51, no. 4, pp. 799–809, Aug. 2004.

[27] H. Tajima and Y. Hori, "Speed sensorless field-orientation control of induction machine," *IEEE Trans. Ind. Appl.*, vol. 29, no. 1, pp. 175–180, Jan. /Feb. 1993.

[28] J. Holtz and J. Quan, "Drift-and parameter-compensated flux estimator for persistent zero-stator-frequency operation of sensorless-controlled induction motors," *IEEE Trans. Ind. Appl.*, vol. 39, no. 4, pp. 1052–1060, Jul./Aug. 2003.

[29] L. Tang, M. F. Rahman, and M. E. Haque, "Low speed performance improvement of a direct torque controlled interior permanent magnet synchronous machine drive," in *Proc. 19th Annu. IEEE APEC*, 2004, vol. 1, pp. 558–564.

[30] N. Mohan, T. M. Undeland, and W. P. Robbins, *Power electronics-Converters, Applications and Design, 2nd* ed., New York: John Wiley & Sons Inc., 1995, pp. 211–244.

[31] Z. Q. Zhu, K. Utaikaifa, K. Hoang, Y. Liu, and D. Howe, "Direct torque control of three-phase PM brushless AC motor with one phase open-circuit fault," in *Proc. IEEE Int. Conf. Electrical Machines and Drives,* May 3–6, 2009, pp. 1408–1415.

[32] Z. Q. Zhu, K. Ng, and D. Howe, "Design and analysis of high-speed brushless permanent magnet motors," in *Eighth International Conference on Electrical Machines and Drives, 1997*, Sept. 1–3, 1997, pp. 381–385.

Khoa D. Hoang (S'10) received the B.Eng and M.Eng degrees from Ho Chi Minh City University of Technology (HCMUT), Ho Chi Minh City, Vietnam, in 2002 and 2005, respectively, all in electrical and electronics engineering.

He is currently working toward the Ph.D. degree in the Department of Electronic and Electrical Engineering, the University of Sheffield, UK. His key research interests include power conversion, electrical machine, and advanced control techniques for electrical drives.

Z. Q. Zhu (M'90–SM'00-F'09) received the B.Eng. and M.Sc. degrees from Zhejiang University, Hangzhou, China, in 1982 and 1984, respectively, and the Ph.D. degree from the University of Sheffield, Sheffield, U.K., in 1991.

Since 1988, he has been with the University of Sheffield, where he is currently a Professor at the Department of Electronic and Electrical Engineering, and Head of the Electrical Machines and Drives Research Group. His current major research interests include design and control of permanent magnet brushless machines and drives, for applications ranging from automotive to renewable energy.

Martin P. Foster received the B.Eng. degree in electronic and electrical engineering, the M.Sc.(Eng.) degree in control systems, and awarded a PhD for his thesis "Analysis and Design of High-order Resonant Power Converters" from the University of Sheffield, Sheffield, U.K., in 1998, 2000, and 2003, respectively. In 2003 he became a member of academic staff at Sheffield specialising in power electronic systems.

His current research interests include the modelling and control of switching power converters, resonant power supplies, multilevel converters, battery management, piezoelectric transformers, power electronic packaging and autonomous aerospace vehicles.